Hyperfine Structure in the Inversion Spectrum of $N^{14}H_3$ by a New High-Resolution Microwave Spectrometer*

J. P. GORDON†
Columbia University, New York, New York
(Received May 4, 1955)

The hyperfine structure of the inversion spectrum of $N^{14}H_3$ has been reexamined with an ultra-high resolution spectrometer. Lines whose total width at half-maximum is seven kc-sec have been obtained in this spectrometer. Such narrow lines allow resolution of magnetic hyperfine structure caused by reorientation of the spins of the hydrogen nuclei. The new structure has been satisfactorily explained to within the experimental error of about 1 kc/sec by considering the various interactions of the magnetic moments of the hydrogen nuclei with the molecular fields. The interaction energy of the nitrogen nucleus has been remeasured with higher resolution than was possible previously, and indications were found that $|eqQ|$ for the lower inversion state is larger by about 0.01% than that for the upper state. The sign of eqQ was directly determined to be negative. A theoretical treatment of the magnetic interactions has been made which is slightly different from that which has previously been used. The method allows some simplification of the form of the magnetic interactions.

INTRODUCTION

THE inversion spectrum of the symmetric top molecule $N^{14}H_3$ has been the subject of a great deal of study ever since it was first observed by Cleeton and Williams in 1934.[1,2] Hyperfine structure in this spectrum due to quadrupole interaction of the nitrogen nucleus was first noticed in 1946 by Good.[3] Quite recently, a thorough theoretical and experimental study of the hyperfine structure of this spectrum has been carried out by Gunther-Mohr *et al.*[4,5] which explained a doubling of the $K=1$ lines in terms of the magnetic interactions of the hydrogen nuclei with the molecular magnetic fields.

A significant increase in experimental resolution afforded by the molecular beam spectrometer described in this paper has made it desirable to remeasure once again in greater detail the hyperfine structure of this spectrum. Previously undetected structure caused by the reorientation of the spins of the hydrogen nuclei has been observed and theoretically explained to within experimental error. The theoretical analysis of Gunther-Mohr *et al.* has been extended to include evaluation of the mutual spin-spin interaction of the three hydrogen nuclei, and simplification of some of the terms of the Hamiltonian has been effected through the use of the symmetry properties of the molecule.

* Work supported jointly by the Signal Corps, the Office of Naval Research, and the Air Research and Development Command.

† Now at the Bell Telephone Laboratories, Inc., Murray Hill, New Jersey.

[1] C. E. Cleeton and N. H. Williams, Phys. Rev. **46**, 235 (1934).

[2] The reader is referred to C. H. Townes and P. Kisliuk, National Bureau of Standards Circular, 518, June 23, 1952 (unpublished), in which will be found a summary of the experimental and theoretical work on this molecule together with a survey of the literature and a tabulation of microwave transition frequencies.

[3] W. E. Good, Phys. Rev. **70**, 213 (1946).

[4] Gunther-Mohr, White, Schawlow, Good, and Coles, Phys. Rev. **94**, 1184 (1954).

[5] Gunther-Mohr, Townes, and Van Vleck, Phys. Rev. **94**, 1191 (1954).

THEORY

The experimental[4] and theoretical[5] papers by Gunther-Mohr *et al.* form the background for the following work. For convenience, they will be referred to as GM I and GM II respectively.

The rotational state of the molecule in zero field will be specified by the following quantum numbers:

- $\mathbf{J}$ total molecular angular momentum excluding nuclear spins.
- K projection of $\mathbf{J}$ on the molecular axis of symmetry.
- $\mathbf{I}_N$ spin of the nitrogen nucleus.
- $\mathbf{I}_i$ ($i=1, 2, 3$) spin of the ith hydrogen nucleus.
- $\mathbf{I}$ sum of the spins of the three hydrogen nuclei.
- $\mathbf{F}_1$ sum of $\mathbf{J}$ and $\mathbf{I}_N$ (this is a good quantum number because the quadrupole interaction energy of the nitrogen is considerably larger than the magnetic interaction energy of the hydrogens).
- $\mathbf{F}$ sum of F_1 and $\mathbf{I}$.
- M_F projection of F on some axis fixed in space.

The calculation of the various matrix elements will be made in the molecular frame coupling scheme, as described by Van Vleck[6] and GM II. The molecular frame scheme is based on the fact that if one refers all angular momenta to set of axes fixed in the molecule, then $\mathbf{F}$, $\mathbf{I}_N$, and $\mathbf{I}$ form a set of commuting angular momenta, just as in the laboratory frame, $\mathbf{J}$, $\mathbf{I}_N$, and $\mathbf{I}$ form a commuting set. In the molecular frame, however, the commutation relations of $\mathbf{F}$ and $\mathbf{F}_1$ change sign: i.e., $[F_x,F_y]=-iF_z$; where x, y, and z now refer to axes fixed in the molecule. The "internal" angular momenta $\mathbf{I}$ and $\mathbf{I}_N$, however, retain the old commutation relations. If one reverses the signs of these internal angular momenta, setting $\mathbf{I}_N'=-\mathbf{I}_N$, $\mathbf{I}'=-\mathbf{I}$, then all of the angular momenta commute with the anomalous sign, and one has the molecular frame coupling scheme

$$\mathbf{F}_1=\mathbf{F}+\mathbf{I}', \quad \mathbf{J}=\mathbf{F}_1+\mathbf{I}_N',$$

[6] J. H. Van Vleck, Revs. Modern Phys. **23**, 213 (1953).

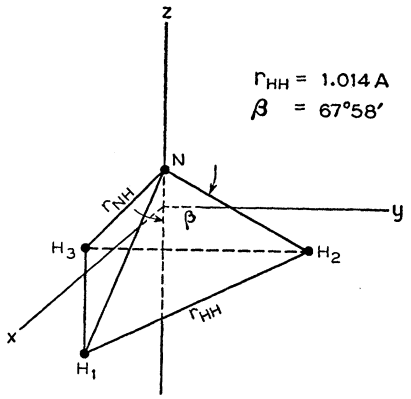

FIG. 1. Geometrical structure of the ammonia molecule.

and such relations as

$$\mathbf{I}'^2=\mathbf{I}^2=I(I+1), \quad \mathbf{F}\cdot\mathbf{I}'=-\mathbf{F}\cdot\mathbf{I}.$$

The matrix elements of Condon and Shortley[7] may be used for this coupling scheme, provided one reverses the signs of all the imaginary ones. The molecular frame has a distinct advantage, for calculations, in that the positions of the nuclei are fixed in the coordinate system (except for vibrations) and it becomes unnecessary to know the matrix elements of the direction cosines which determine the angular position of the molecule in space.

The interactions which are important in the hyperfine structure of the inversion spectrum of ammonia are listed in Table I.[8] They include the effects previously evaluated in GM II, with the addition of the mutual spin-spin interaction of the magnetic moments of the hydrogen nuclei. The reader is referred to GM I and GM II for the evaluation of any constants not explicitly defined here. The combined effect of these interactions satisfactorily fits almost all the experimental data to within the accuracy of measurement. The few apparent discrepancies which still remain will be discussed later.

We shall proceed to a calculation of the hydrogen spin-spin interaction. Reference should be made to Fig. 1 which shows the structure of the molecule and the positions of the nuclei with respect to the molecular axes. The z axis is the axis of symmetry of the molecule, the xz plane contains hydrogen No. 1, and the projection of the position of hydrogen No. 2 on the xy plane lies in its second quadrant. The origin of the coordinate system is taken at the center of gravity of the molecule. The x, y, and z axes form a right-handed set of coordinates.

[7] E. U. Condon and G. H. Shortley, *Theory of Atomic Spectra* (Cambridge University Press, London, 1951).

[8] Some errors noticed in GM I and GM II are corrected here and in Eq. (5). These errors include: (*a*) The function f of Eq. (5) is written incorrectly in GM II. (*b*) in GM I and II, the magnetic constants α and ρ should be replaced in all equations by $\alpha/2$ and $\rho/2$. These constants, of course, keep the same definitions as before. (*c*) in GM II, Appendix III, Eq. (A23), the proportionality constant $\Omega_1(J,I_N)/[J(J+1)]$ should be replaced by $\varphi(J,I_N')/[J(J+1)]$ where $\varphi(J,I_N')=2\Omega_2(J,I_N)-\mathbf{I}_N\cdot\mathbf{J}$.

The energy of the spin-spin interactions among the three hydrogen nuclei is given by[9]

$$G_1^{HH}=(g_H\mu_0)^2 r_{HH}^{-3} \times\sum_{i<j}[\mathbf{I}_i\cdot\mathbf{I}_j-3r_{HH}^{-2}(\mathbf{I}_i\cdot\mathbf{r}_{ij})(\mathbf{I}_j\cdot\mathbf{r}_{ij})], \quad (1)$$

where r_{HH} is the distance between hydrogen nuclei, and $\mathbf{r}_{ij}$ is the vector distance between hydrogen nuclei i and j. As shown in the Appendix, the only matrix elements of this interaction which affect the spectrum in an observable way are those which are diagonal in K, and if only these elements are considered, it is shown there that the interaction can be written in the equivalent form:

$$G_1^{HH}=-\tfrac{1}{4}(g_H\mu_0)^2 r_{HH}^{-3}(\mathbf{I}^2-3\mathbf{I}_z^2), \quad (2)$$

where I_z is the projection of I on the molecular symmetry axis. This term may then be evaluated in a similar way to that by which the term $(\mathbf{I}_{Nz}^2-\mathbf{I}_N^2/3)$ is evaluated in GM II, giving the result:

$$G_1^{HH}=-\tfrac{1}{4}(g_H\mu_0)^2\langle v|r_{HH}^{-3}|v\rangle \times\frac{\varphi(F_1,I')\varphi(J,F_1)}{F_1(F_1+1)}\left(1-\frac{3K^2}{J(J+1)}\right), \quad (3)$$

TABLE I. Interactions important in the hyperfine structure of the inversion spectrum of $N^{14}H_3$.

Energy term	Physical interpretation
$-eqQ\left(1-\frac{3K^2}{J(J-H)}\right)\Omega_1(J,I_N)$	Nitrogen quadrupole interaction
$\left[a+\frac{(b-a)K^2}{J(J+1)}\right](\mathbf{I}_N\cdot\mathbf{J})$	Nitrogen magnetic interaction with molecular rotation
$\left[A+\frac{cK^2}{J(J+1)}-\delta_{K1}(-1)^{J+v}B\right](\mathbf{I}\cdot\mathbf{J})$	Hydrogen magnetic interaction with molecular rotation
$g_H g_N\mu_0^2 r_{NH}^{-3}\sum_{i=1,2,3}[(\mathbf{I}_i\cdot\mathbf{I}_N)-3(\mathbf{I}_i\cdot r_{iN})(\mathbf{I}_N\cdot\mathbf{r}_{iN})]$ or $\mathfrak{D}_1(\mathbf{I}\cdot\mathbf{I}_N-3I_zI_{Nz})+3\mathfrak{D}_2(I_{1y}I_{Ny}-I_{1z}I_{Nx})$	Hydrogen-nitrogen spin-spin interaction
$(g_H\mu_0)^2 r_{HH}^{-3}\sum_{i<j}[\mathbf{I}_i\cdot\mathbf{I}_j-3(\mathbf{I}_i\cdot\mathbf{r}_{ij})(\mathbf{I}_j\cdot\mathbf{r}_{ij})]$ or $-\tfrac{1}{4}\mathfrak{D}_3(I^2-3I_z^2)$, where $\mathfrak{D}_1=g_H g_N\mu_0^2\langle v|r_{NH}^{-3}(1-\frac{3}{2}\sin^2\beta)|v\rangle$, $\mathfrak{D}_2=g_H g_N\mu_0^2\langle v|r_{NH}^{-3}\frac{3}{2}\sin^2\beta|v\rangle$, $\mathfrak{D}_3=(g_H\mu_0)^2\langle v|r_{HH}^{-3}|v\rangle$, $A=\frac{1}{2}(\alpha+\rho)$, $B=\frac{1}{2}(\rho-\alpha)$, $C=\gamma-\frac{1}{2}(\alpha+\rho)$;	Hydrogen-hydrogen spin-spin interaction

α, ρ, and γ are proportional to the magnetic fields at the position of hydrogen nucleus 1 (see Fig. 1) caused by rotations of the molecule about the x, y, and z axes, respectively (see GM II).

[9] The notation here for the Hamiltonian is patterned after GM II.

where $\langle v|r_{HH}^{-3}|v\rangle$ indicates that r_{HH}^{-3} is to be averaged over the inversion, and

$$\varphi(A,B)=\frac{6(\mathbf{A}\cdot\mathbf{B})^2-3(\mathbf{A}\cdot\mathbf{B})-2A(A+1)B(B+1)}{(2A+3)(2A-1)}. \quad (4)$$

It can be shown from symmetry arguments that the total hydrogen spin depends on K, so that when K is a multiple of 3, I is $\frac{3}{2}$, while for all other values of K, $I=\frac{1}{2}$. Since states with $I=\frac{1}{2}$ must have $I_z^2=\frac{1}{4}$, it can be seen from Eq. (2) that G_1^{HH} is zero in this case. Thus this interaction does not affect the hyperfine structure of the energy levels unless K is a multiple of three. When K is a multiple of three, however, it forms an important component of the magnetic structure. In computing the magnitude of the coupling constant $(g_H\mu_0)^2\langle v|r_{HH}^{-3}|v\rangle$ we have used for $\langle v|r_{HH}^{-3}|v\rangle$ merely the inverse cube of the equilibrium value of r_{HH} which was obtained using the values given by Herzberg[10] for the hydrogen nitrogen distance r_{HH} and the apex angle β which are illustrated in Fig. 1. These values are $r_{HH}=1.014\times10^{-8}$ cm, $\beta=67°58'$. The coupling constant was thus calculated to be 27.7 kc/sec, and this value provides a good fit to the experimental spectrum.

Combining this result with those of GM II, we arrive at the final form of the complete hyperfine energy. This equation is valid, as explained below, so long as the quadrupole energy term is large compared to the magnetic terms.

$$\begin{aligned}W_{JJKF_1F}=&-\langle v|eQq|v\rangle\left(1-\frac{3K^2}{J(J+1)}\right)\Omega_1(J,I_N)\\&+\left[a+\frac{(b-a)K^2}{J(J+1)}\right](\mathbf{I}_N\cdot\mathbf{J})\\&+\left[A+\frac{CK^2}{J(J+1)}\right]\frac{(\mathbf{I}\cdot\mathbf{F}_1)(\mathbf{F}_1\cdot\mathbf{J})}{F_1(F_1+1)}\\&+2g_Hg_N\mu_0^2\langle v|r_{HH}^{-3}(1-\tfrac{3}{2}\sin^2\beta|v\rangle\\&\times\frac{(\mathbf{F}_1\cdot\mathbf{I})\Omega_2(J,I_N)}{F_1(F_1+1)}\left(1-\frac{3K^2}{J(J+1)}\right)\\&-\tfrac{1}{4}(g_H\mu_0)^2\langle v|r_{HH}^{-3}|v\rangle\frac{\varphi(F_1,I')\varphi(J,F_1)}{F_1(F_1+1)}\\&\times\left(1-\frac{3K^2}{J(J+1)}\right)-\delta_{K1}(-1)^{J+5}2\mathbf{F}, \quad (5)\end{aligned}$$

where

$$\begin{aligned}2f=&\langle v|r_{HH}^{-3}\tfrac{3}{2}\sin^2\beta|v\rangle 2g_Hg_N\mu_0^2\\&\times\frac{(\mathbf{F}_1\cdot\mathbf{I})\Omega_2(J,I_N)}{F_1(F_1+1)}+B\frac{(\mathbf{I}\cdot\mathbf{F}_1)(\mathbf{F}_1\cdot\mathbf{J})}{F_1(F_1+1)},\end{aligned}$$

[10] G. Herzberg, *Infra-Red and Raman Spectra* (D. Van Nostrand and Company, Inc., New York, 1945).

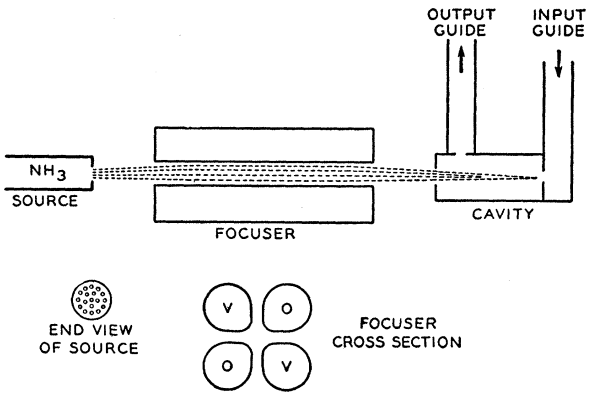

FIG. 2. Block diagram of the molecular beam oscillator.

$$\Omega_1(J,I_N)=\frac{3(\mathbf{I}_N\cdot\mathbf{J})^2+\frac{3}{2}(\mathbf{I}_N\cdot\mathbf{J})-I_N(I_N+1)J(J+1)}{(2J-1)(2J+3)2I_N(2I_N-1)},$$

$$\Omega_2(J,I_N)=\frac{3(\mathbf{I}_N\cdot\mathbf{J})^2+2J(J+1)(\mathbf{I}_N\cdot\mathbf{J})-I_N(I_N+1)J(J+1)}{(2J-1)(2J+3)}.$$

In addition to this expression, the magnetic terms of Table I have matrix elements off diagonal in F_1 which might be expected to contribute measurable shifts in some of the lines where the quadrupole splittings are small. For the 3–2 line, in particular, the factor $[1-3K^2/J(J+1)]$ is equal to zero, so that the quadrupole coupling energy disappears, F_1 is no longer a good quantum number, and expression 5 is no longer valid. Of the lines we measured, the largest effect of terms off-diagonal in F_1 appears in the 4–3 line, since for this line the quadrupole splittings were small and the magnetic energies large. In this case some of the individual hyperfine structure components are shifted by as much as two kc/sec, but this did not produce a detectable change in the envelope of all components of the lines.

EXPERIMENTAL CONSIDERATIONS

The experimental results were obtained by use of an ultra-high resolution spectrometer.[11] A block diagram of this spectrometer is shown in Fig. 2. Ammonia gas at room temperature is maintained in the source at 5 to 20 mm pressure. Molecules emerge from the source through a group of fine tubes and travel through an electrostatic focuser in which a highly nonlinear electric field focuses the molecules which are in upper inversion states. Molecules in lower inversion states are defocused and so removed from the beam. The beam then traverses a high-Q resonant cavity tuned to an inversion frequency, and there transitions are induced by microwave radiation from a 2K50 klystron. We shall discuss here only those properties of the apparatus which are necessary

[11] Gordon, Zeiger, and Townes, Phys. Rev. **95**, 282 (1954).

to an understanding of the spectroscopic results. A more general and complete discussion, including the properties of the apparatus as a microwave amplifier and oscillator, is given in the following paper.

Most attempts by previous workers to utilize a molecular beam for microwave spectroscopy have failed to be very successful because of a lack of sensitivity. The electrostatic focuser used here, allows both a sizeable beam, and large signals from a given number of molecules in the beam. Consider first a gas in thermal equilibrium which is irradiated by microwaves at the frequency of one of the transitions of the gas molecules. An absorption of energy invariably takes place. There will be molecules in both the higher and lower energy states of the transition, and the microwaves will excite transitions both up and down with equal probability. The total rate of upward transitions will, however, be slightly larger than the rate of downward transitions, since the Boltzmann distribution gives the lower state a population larger than the upper by approximately $N(h\nu/kT)$, where N is the total number of molecules in the lower state. For $T=300°$K, $kT/10^6$h equals 6.63 $\times 10^6$ Mc/sec, and so $h\nu/kT$ is approximately 1/250 at the frequency of 1.25-cm microwaves. At this frequency, then, the net effect is produced by only 1/250 of the molecules which are capable of absorbing energy. In the present apparatus, only molecules in upper inversion states reach the cavity. Since they can all contribute energy to the exciting microwave field, there results a substantial improvement in the sensitivity of the apparatus. The fact that the upper inversion states are focused means that the molecular response to the exciting radiation is an emission of energy, so that emission lines are observed rather than absorption lines.

Cylindrical cavities were used, which resonated in the TE_{011} mode at the frequency of interest. In order to provide a long interaction region and so to cut down the line width (this is discussed in detail in the following paper), the cavities were made approximately four inches in length. They were tuned by means of short sections of enlarged diameter and variable length at one end. The beam entered through a circular hole in the other end. In order to make cavities of this length for the TE_{011} mode, their diameters had to be very close to the cut-off values. This restricted the tuning range of each cavity to about 50 Mc/sec, and so a new cavity usually had to be constructed for each line which was examined. The cavities were made of copper and had values of Q near 12 000. Suprisingly little radiation from the beam entrance hole was encountered, even though the hole diameter was two thirds of the diameter of the cavity.

Emission lines whose total width at half-maximum is seven kc/sec have been obtained, and it is estimated that from two to four kc/sec of this width is due to spurious frequency modulation of the microwave signal from the 2K50 klystron which was used to induce the transitions, rather than to the actual width of the spectral lines.

The field of the focuser exerts forces on the molecules due to their induced dipole moments. In zero field the ammonia molecule has no average dipole moment because of the inversion, while with increasing field, the inversion is slowly quenched and an average dipole moment appears. If hyperfine effects are neglected the energies of the inversion states may be written for all field strengths as

$$W=W_0\pm\left[\left(\frac{h\nu_0}{2}\right)^2+\left(\mu\mathcal{E}\frac{MK}{J(J+1)}\right)^2\right]^{\frac{1}{2}}, \qquad (6)$$

where W_0 is the average energy of the upper and lower inversion levels, ν_0 is the inversion frequency in zero electric field, μ is the permanent dipole moment the molecule would have if the inversion did not occur, $\mathcal{E}$ is the magnitude of the electric field, and M is the projection of J on the direction of the field. Since the changes in magnitude and direction of the field the molecule sees as it travels through the focuser occur very slowly compared to the rate of precession of J around the field, J maintains its orientation with respect to the field direction during the whole flight of of the molecule. Therefore M is a constant of the motion.

The focuser, as shown in Fig. 2, is composed of four cylindrical electrodes whose inner faces are shaped to form hyperbolae. Two opposing electrodes are maintained at a high voltage V, while the other two are kept at ground. This arrangement produces an electric potential in the gap between the electrodes of the form $\varphi=\varphi_0 r^2\cos 2\theta$; where r and θ are cylindrical coordinates of a system whose axis is the axis of the focuser. The magnitude of the electric field produced by this potential is proportional to r. The force exerted on the molecules by this field is, from (6),

$$f_r=-\frac{\partial W}{\partial r}=\mp\frac{[\mu MK/J(J+1)]^2\mathcal{E}d\mathcal{E}/dr}{\{(h\nu_0/2)^2+[\mu\mathcal{E}MK/J(J+1)]^2\}^{\frac{1}{2}}}. \qquad (7)$$

It is radial and proportional to r for small field strengths. The force is directed inward for molecules in upper inversion states (negative sign) and outward for molecules in lower inversion states (positive sign).

Under the assumption of small electric fields, the number of molecules in the upper state and with a given value of M which are held in the focuser by the restoring force is approximately proportional to M^2. This can be seen as follows. Assume that the source consists of a small hole located on the axis of the focuser from which molecules effuse in all directions. Assume further that all molecules which can travel farther away from the axis of the focuser than a distance of r_0 collide with the focuser electrodes and are lost from the beam. It can easily be shown that all molecules whose initial velocity perpendicular to the axis of the focuser is less than a

given v_{m0} are kept within the focuser, where v_{m0} is proportional to M. For any axial velocity v_z, all molecules in a given M state which emerge from the source within a solid angle $\Omega_M=\pi(v_{m0}/v_z)^2$ are thus kept within the focuser, and since v_{m0} is proportional to M, Ω_M is proportional to M^2. Since Ω_M is small, the number of molecules in solid angle Ω_M is proportional to Ω_M, and thus to M^2. Actually none of the assumptions made here is exactly correct, the principal deviation being due to the decrease in polarizability of the molecule at strong fields. However, calculations show that the results are not changed by this effect in a very important way. Hence we shall assume for simplicity, that the field is relatively weak ($\mu\mathcal{E}\ll h\nu_0$), so that the number of upper state molecules trapped by the potential minimum of the focuser, and thus delivered to the cavity, is proportional to M^2.

We shall see that as the molecules enter, traverse, and leave the focuser, very few transitions are made between the various quadrupole levels of a given inversion state. This fact plus the dependence of the focusing strength on M will be shown to have the effect of substantially increasing the relative populations of the higher energy quadrupole levels inside the cavity. The quadrupole satellites on the high-frequency side of the main line are made relatively strong by this effect.

Neglecting for a moment the effects of the hydrogen spins, we see that in small electric fields, J and the nitrogen spin I_N are coupled together by the quadrupole interaction and the stationary states of the molecule may be represented by the quantum numbers J, I_N, F_1, and M_F, where $\mathbf{F}_1=\mathbf{J}+\mathbf{I}_N$ and M_F is the projection of $\mathbf{F}_1$ along the direction of the field. At high fields, $\mathbf{J}$ and $\mathbf{I}_N$ are decoupled and separately quantized along the field direction. At all intermediate fields, the stationary states have a one to one correspondence with the low- or high-field states. If a molecule exists at low field in a particular quantum state and then the field is increased infinitely slowly (adiabatic approximation) the state of the molecule will progress through the intermediate configurations and at high field will be found in a particular high-field state. If the field is turned on within a finite time, then transitions will be possible, and the molecule may then be found in any of several high-field states.

The criterion for whether such transitions will take place is discussed in most textbooks on quantum mechanics. Let $\hbar\omega_{km}$ be the energy difference between states k and m. Then if there is only a small fractional change in $\hbar\omega_{km}$ in a time given by $1/\omega_{km}$, few transitions between states k and m are to be expected. The most probable velocity of the ammonia molecules in the beam is about 4×10^4 cm/sec and the distance they travel in entering or leaving the focuser is about one centimeter, so that they take about 2.5×10^{-5} second to enter the field. The quadrupole level splittings are of the order of 1.5 Mc/sec, so that for transitions to occur between these levels, the energy differences between quadrupole states must undergo large fractional changes in times of the order of $[2\pi\times1.5\times10^6]^{-1}$ or about 10^{-7} sec. This time is short, however, compared to the time required for the molecule to enter or leave the fields, so that we should expect few transitions.

In addition, each of the quadrupole levels is further split in zero field by the magnetic interactions of the hydrogen spin, which are listed in Table I. These zero field magnetic hyperfine splittings are only of the order of 50 kc/sec, however, so that in the case of these energy splittings the time $1/\omega_{km}$ is of the same order as the time of entry of the molecules into the focuser. We should thus expect many transitions between these levels, and in our computing theoretical line shapes, we have assumed that in the cavity all the magnetic hyperfine sublevels of a given quadrupole level are equally populated.

As an example of the intensity shifts produced by adiabatic focusing we shall take the case of the 3–3 line, which is one of those experimentally measured. Since eqQ is negative, Eq. (5) shows that the $F_1=3$ state has the highest energy, followed by the $F_1=4$ and 2 states respectively. Of the seven low-field M_F states with $F_1=3$, four go at high fields to $|M|=3$ states, two to $|M|=2$, and one to $|M|=1$. The other low-field states are somewhat similarly distributed among the high-field states. However, there is a significant trend for low-energy low-field states to go predominantly into the low-energy high-field states. Following our assumption that the number of molecules in a given M state which reach the cavity is proportional to M^2, the population of each F_1 level in the cavity must be weighted according to the factor $(2F_1+1)^{-1}\sum_M N(M)M^2$, where $N(M)$ is the number of low-field states which go into the particular high-field state with quantum number M. For the 3–3 line, these weighting factors are 45/7, 37/9, and 2/5 respectively for the states $F_1=3$, 4, and 2. The high-energy quadrupole levels thus have substantially greater populations in the cavity. The relative intensities of the transitions originating from the various quadrupole levels must be weighted by these factors.

The effect of this varying of the weight-factor was experimentally observed as a variation in intensity of the transitions. Under conditions of thermal equilibrium, the hyperfine pattern of the 3–3 line should be almost exactly symmetrical intensitywise, and in particular the two transitions $F_1=3\rightarrow2$ and $F_1=2\rightarrow3$ equal in intensity. Actually, while the $F_1=3$ to 2 quadrupole satellite was quite strong (see Fig. 4), the $F_1=2$ to 3 quadrupole satellite on the low frequency side of the main line was just barely observable.

The relative intensities of the quadrupole satellites were used to provide a direct check on the sign of eqQ. Under the correct assignment of a negative eqQ, both quadrupole satellites on the high frequency side of the main line originate from the same quadrupole level and thus their relative intensities are unchanged by the

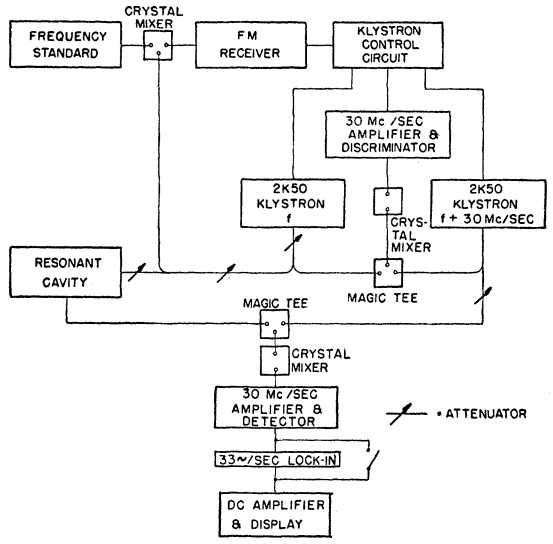

FIG. 3. Block diagram of the heterodyne detection system used in the experimental work.

adiabatic focusing, while the quadrupole satellites on the low frequency side originate from different quadrupole levels, and so have different intensities. The $K=1$ line also checked the sign of eqQ, since the details of its asymmetric hyperfine structure depend on the relative sign of eqQ and the nuclear spin-spin interaction. The sign of the latter interaction is of course known from the nuclear magnetic moments. This determination also shows that eqQ is negative.

The large changes in the relative populations of the quadrupole levels due to focusing also allow the possibility of producing direct quadrupole transitions in the beam in the region between the focuser and the cavity. The cavity would then be used as a detector, the quadrupole resonances being observed by the changes in intensity of the quadrupole satellites of the microwave transitions.

ELECTRONICS AND MEASUREMENT TECHNIQUE

A block diagram of the heterodyne detection system used in this work appears in Fig. 3. The carrier power from the signal klystron $K1$ plus power emitted from the beam is mixed in a 1N26 crystal with power from a second klystron $K2$ which is maintained by an automatic frequency control AFC circuit at a frequency 30 Mc/sec away from that of $K1$. A tuned intermediate-frequency (IF) amplifier with a band width of about 2.5 Mc/sec then amplifies the resulting 30-Mc/sec signal. The output of this amplifier is detected in a diode second detector, and then fed through a low-pass filter to an oscilloscope. Alternatively, the output from the second detector may be sent to a 33-cps lock-in detector which is synchronized with mechanical beam chopper inside the vacuum system.

Most of the measurements were taken without the lock-in circuit. Klystrons $K1$ and $K2$ were frequency-modulated by applying to their repellers a sawtooth sweep voltage at a rate of about 20 cps from an oscilloscope. The output of the diode second detector was then fed through a low pass filter with a bandpass of about 200 cps, and displayed on the scope. The emission lines appeared on the scope, as in Fig. 4 when the klystron $K1$ swept through the ammonia transition frequencies.

The line frequencies were measured in the usual way by means of standard frequency markers at 30-Mc/sec intervals generated by multiplication up from a 50-kc/sec quartz crystal oscillator whose frequency is monitored directly against radio station WWV.[12] An AM receiver tuned to the frequency difference between the ammonia line frequency and the nearest standard marker picks up the beat note between the signal klystron and the standard marker. As the klystron sweeps, a pip emerges from the receiver which is displayed on the oscilloscope along with the emission line pattern. Calibration of the receiver setting gives the line frequency when the pip is centered on the line.

The lock-in detector was also used during a few of the frequency measurements. In this case the difference between the signal klystron frequency and a nearby standard frequency was fed into an FM reciver, and the discriminator output of the receiver was used as an AFC to fix the frequency of the signal klystron at a point determined by the receiver tuning. Point by point measurements at intervals of a few kilocycles were then made in order to take advantage of the long time-constants (about $\frac{1}{3}$ sec) afforded by the lock-in circuit. The increase in sensitivity afforded by the reduced band width of the lock-in system was, however, offset by a decrease in resolution caused by the introduction of spurious frequency modulation into the klystron signal from noise in the frequency standard. In addition this method was considerably more cumbersome and time-consuming and hence was not used very much.

The equivalent band with for a detecting system of the type used has been discussed by Geschwind,[13] who showed that it is

$$\Delta\nu=[(\Delta\nu_1)(\Delta\nu_2)]^{\frac{1}{2}},$$

where $\Delta\nu_1=2.5\times10^6$ cps is the band width of the IF amplifier, and $\Delta\nu_2$ is the band width of the output circuit of the diode second detector. In the first and most frequently used measuring technique discussed above, $\Delta\nu_2$ was about 200 cps, so that

$$\Delta\nu=(2.5\times10^6\times2\times10^2)^{\frac{1}{2}}=2.2\times10^4 \text{ cps}.$$

An increased signal-to-noise ratio is therefore possible if the band width of the detecting system is reduced.

[12] Gordy, Smith, and Trambarulo, *Microwave Spectroscopy* (John Wiley and Sons, Inc., New York, 1953).

[13] S. Geschwind, thesis, Columbia University, 1951 (unpublished). See also Ann. N. Y. Acad. Sci. **55**, 751 (1952), Article 5.

The measurements were made difficult by the width of the frequency standard marker pips. This width is caused by spurious frequency modulation of the standard and klystron signals. At best, the marker pips could be narrowed to about 10 or 15 kc/sec, and the center of the pips could only be determined to about 1 kc/sec. The situation, plus the fact that drifts in the klystron control circuits made it difficult to keep the lines on the scope for very long, made the measurements accurate only to about one kilocycle, or about one seventh of the line width. In addition, most of the lines measured were unresolved structures whose shapes could not be accurately calculated because of the effects of the focuser on the populations of the various hyperfine levels. Thus, while measurements could be repeated to an accuracy of about 1 kc/sec, errors in the determinations of the positions of incompletely resolved lines were perhaps somewhat greater. The theoretical frequencies listed in Table II represent our best estimate of the frequencies determined from the theoretical patterns, which should correspond to the measured frequencies.

THE MEASUREMENTS

Measurements were taken on the hyperfine structure of the 1–1, 2–2, 3–3, and 4–3 lines of the NH_3 inversion spectrum. These measurements allowed accurate experimental values to be obtained for the constants A and C of the hydrogen magnetic interaction [see Eq. (5)]. They also provided accurate checks on the previously determined magnetic constants B, a, and b, and of the quadrupole coupling constant eqQ and its dependence on J and K. A slight asymmetry of the hyperfine structure of the 3–3 line was observed and explained by assuming that the magnitude of eqQ is 4 ± 1 kc/sec larger in the lower inversion state than in the upper; however, an apparent slight asymmetry in the structure of the 4–3 line is still unexplained.

Best values for the magnetic constants are, in kc/sec,

$$A=-17.3\pm0.5,\quad B=-14.1\pm0.3,\quad C=-2.0\pm1.0,$$
$$a=6.66\pm0.2,\quad b=6.66\pm0.2,$$

and the quadrupole coupling constant is given by

$$\langle eqQ\rangle_{Av}=4089\{1+7.7\times10^{-5}[J(J+1)+K^2]\}\pm1.5 \text{ kc/sec},$$

where $\langle eqQ\rangle_{Av}$ is the average of the quadrupole coupling constants for the upper and lower inversion levels. This result was chosen to provide a best fit to both our data and those of GM I. Our own data on the relatively low J and K lines are somewhat better fitted by a formula

$$\langle eqQ\rangle_{Av}=-4092.4[1+5\times10^{-5}J(J+1)]\pm1.5 \text{ kc/sec},$$

which, however, does not agree well at high J and K with the results of GM I.

The magnetic structures of the inversion lines may be divided into two classes; those for which $K=1$, and those for which $K\neq1$. For the latter case the K degeneracy (this is discussed in some detail in GM II) is not lifted by the hyperfine interactions. Hence the hyperfine structure of the upper and lower inversion levels is almost identical, and so the hyperfine structure of lines with $K\neq1$ is almost symmetrical about the position of a line undisplaced by hyperfine structure. The only departure from symmetry for which we have allowed is the difference in the quadrupole coupling constants for the upper and lower inversion states.

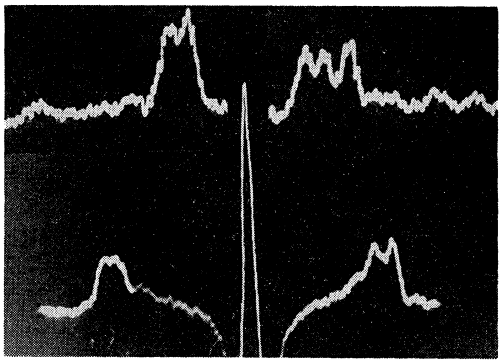

FIG. 4. Composite oscilloscope photograph of the $N^{14}H_3$ $J=K=3$ inversion transition at 23 870 Mc/sec. Below: main line with satellites caused by reorientation of the hydrogen spins. Above left: Inner quadrupole satellite, showing structure due to the hydrogens. Above right: outer quadrupole satellite. The main line has been retouched to make it more visible in the reproduction.

Figures 4 and 5 show the experimental and theoretical structures, respectively, of the 3–3 line. This is the most intense of the observed lines and is an example of the structure to be expected for the $K\neq1$ lines. The main line, composed of the twelve individual hyperfine transitions for which $\Delta F=\Delta F_1=0$, is closely flanked on either side by the magnetic satellites. The satellite on the high-frequency side of the main line is composed of the nine transitions for which $\Delta F=+1$, $\Delta F_1=0$, while the one on the low frequency side has $\Delta F=-1$, $\Delta F_1=0$. At frequency intervals of 1.7 and 2.3 Mc/sec on either side of the main line lie the quadrupole satellites, each of which as its own magnetic structure. This magnetic hyperfine structure of both the main line and the quadrupole satellites had not previously been observed due to lack of resolution or sensitivity. Because of the adiabatic focusing, the quadrupole satellites on the low-frequency side of the main line are considerably weaker than those on the high-frequency side, and only the upper two are shown in Fig. 4. It is to be noticed that the slight asymmetry of the magnetic satellites of the main line is well accounted for by the assumed variation of the quadrupole coupling constant.

Figure 6 shows the theoretical pattern for the 1–1 line. Because of the removal of the K degeneracy by the magnetic interactions in this case, the symmetry of the structure has disappeared. This line was weaker than any of the others, so somewhat larger experimental errors were incurred. It is the only one of the $K=1$ lines which was measured.

TABLE II. Hyperfine spectrum of NH_3. Frequencies are given in kc/sec relative to a theoretical line undisplaced by hyperfine structure. The theoretical frequencies listed are best estimates of the measured positions, after allowances for the observed line shapes and the width of the frequency standard pips.

Component	Transitions $F_1F-F_1'F'$	Experimental frequency	Theoretical frequency
$J=1$, $K=1$; $A+\frac{1}{3}C=-18.3\pm0.3$ kc/sec, $B=-14.1\pm0.3$ kc/sec			
Main line	$2, 5/2 \rightarrow 2, 5/2$ $1, \frac{3}{2} \rightarrow 1, \frac{3}{2}$ $2, \frac{3}{2} \rightarrow 2, 5/2$ $1, \frac{1}{2} \rightarrow 1, \frac{3}{2}$	−15.6	−14.8
	$2, \frac{3}{2} \rightarrow 2, \frac{3}{2}$ $2, 5/2 \rightarrow 2, \frac{3}{2}$ $1, \frac{3}{2} \rightarrow 1, \frac{1}{2}$ $1, \frac{1}{2} \rightarrow 1, \frac{1}{2}$	13.7	13.0
Inner quadrupole satellites	$2, \frac{3}{2} \rightarrow 2, \frac{1}{2}$	−624.2	−622.9
	$2, 5/2 \rightarrow 1, \frac{3}{2}$	−591.3	−590.6
	$2, \frac{3}{2} \rightarrow 1, \frac{3}{2}$ $1, \frac{1}{2} \rightarrow 2, \frac{3}{2}$ $1, \frac{3}{2} \rightarrow 2, \frac{3}{2}$	575.2	572.6
	$1, \frac{3}{2} \rightarrow 2, 5/2$	619.2	617.8
Outer quadrupole satellites	$0, \frac{1}{2} \rightarrow 1, \frac{1}{2}$		1569.0
	$0, \frac{1}{2} \rightarrow 1, \frac{3}{2}$		1526.9
	$1, \frac{1}{2} \rightarrow 0, \frac{1}{2}$ $1, \frac{3}{2} \rightarrow 0, \frac{1}{2}$	1540.3	1540.8

Component	Transitions	No. individual contributing lines	Experimented frequency	Theoretical frequency
$J=2$, $K=2$; $A+\frac{3}{4}C=-18.6\pm0.2$ kc/sec				
Main line	$\Delta F_1=\Delta F=0$	6	+0.3	−0.3
Magnetic satellites	$\Delta F_1=0, \Delta F=-1$	3	−42.2	−42.0
	$\Delta F_1=0, \Delta F=+1$	3	41.1	40.7
Inner quadrupole satellites	$F_1=3 \rightarrow 2, \Delta F=-1$	2	−1297.3	−1297.3
	$F_1=3 \rightarrow 2, \Delta F=0$	1		−1255
	$F_1=2 \rightarrow 3, \Delta F=0$	1	1255.2	1256.0
	$F_1=2 \rightarrow 3, \Delta F=+1$	2	1296.5	1296.6
Outer quadrupole satellites	$F_1=1 \rightarrow 2, \Delta F=0$	1		−2099.8
	$F_1=1 \rightarrow 2, \Delta F=+1$	2	−2056.4	−2057.5
	$F_1=2 \rightarrow -1, \Delta F=-1$	2	2056.8	2057.5
	$F_1=2 \rightarrow 1, \Delta F=0$	1	2100.6	2099.8

Component	Transitions	No. individual contributing lines	Experimented frequency	Theoretical frequency
$J=3$, $K=3$; $A=\frac{3}{4}C=-18.8\pm0.2$ kc/sec				
Main line	$\Delta F_1=\Delta F=0$	12		−0.5
Magnetic satellites	$\Delta F_1=0, \Delta F-1$	9	−71.0	−71.0
			−62.5	−62.5
	$\Delta F_1=0, \Delta F=+1$	9	60.9	61.0
			70.4	70.3
Inner quadrupole satellites	$F_1=4 \rightarrow 3, \Delta F=0$	3		
	$F_1=4 \rightarrow 3, \Delta F=-1$	4		−1689.4
				−1680.0
	$F_1=3 \rightarrow 4, \Delta F=+1$	4	1680	1679.2
			1689.0	1688.6
	$F_1=3 \rightarrow 4, \Delta F=0$	3		
Outer quadrupole satellites	$F_1=2 \rightarrow 3, \Delta F=0$	3		−2365.3
				−2383.8
	$F_1=2 \rightarrow 3, \Delta F=+1$	4		−2323.5
				−2311.2
				−2302.1
	$F_1=3 \rightarrow 2, \Delta F=-1$	4	2303.0	2302.1
			2311.0	2311.2
			2323.0	2323.5
	$F_1=3 \rightarrow 2, \Delta F=0$	3	2365.0	2364.8
			2383.5	2383.0
$J=4$, $K=3$; $A+0.45C=-18.2\pm0.2$ kc/sec				
Main line	$\Delta F=\Delta F_1=0$	12	−1.7	0
Magnetic satellites	$\Delta F_1=0, \Delta F=-1$	9	−82.0	−81.5
			−65.5	−65.5
	$\Delta F_1=0, \Delta F=+1$	9	64.8	65.5
			81.6	81.5
Inner quadrupole satellites	$F_1=5 \rightarrow 4, \Delta F=-1$	3	−460.9	−462.4
	$F_1=4 \rightarrow 5, \Delta F=+1$	3	−464.2	462.6
Outer quadrupole satellites	$F_1=3 \rightarrow 4, \Delta F=+1$	3	−638.4	638.0
	$F_1=4 \rightarrow 3, \Delta F=-1$	3	638.8	638.2

Table II is a list of all the experimentally measured frequencies, along with the corresponding frequencies determined from theoretical plots of the line structures. In most cases, the observed structures were the envelopes of groups of unresolved or partially resolved individual lines. If these structures had several resolved peaks, then wherever possible the positions of the various peaks were measured. In cases where the envelope was a weak unresolved asymmetric structure, the measurement usually corresponded more nearly to the midpoint between the two frequencies at which the emission was at half-maximum rather than to the point of maximum emission. This was so since the width of the frequency standard pip used for measuring was as broad or broader than the line structures involved, and such a piper could be much more easily centered between the steeply sloping sides of a peak than on its relatively indistinct maximum. In some cases errors greater than one kc/sec could be expected, since effects of the adiabatic focusing on the populations of the various hyperfine levels could not be exactly calculated, therefore the calculation of the line shapes for the unresolved structures was subject to some error.

From the spacings of the magnetic satellites of each of the three measured $K\neq1$ lines, values of the quantity $\{A+CK^2/[J(J+1)]\}$ could be obtained to an accuracy of about 0.2 kc/sec. These values are shown in Table II. From them the values of A and C given above were calculated. A best fit was then found for the 1–1 line using these values of A and C and varying B. The value of B so obtained is also given above. Theoretically $\{A+CK^2/[J(J+1)]\}$ and B could both be obtained

from the structure of this line, but since its intensity was small and the errors correspondingly large, it seemed better to determine A and C from the other lines.

Constants for the magnetic energy associated with orientation of the hydrogen nuclei were used to calculate the structures of the quadrupole satellites, and to obtain the positions of lines displaced only by the hyperfine interactions of the nitrogen nucleus. These displacements were then used to calculate values of $\langle eqQ\rangle_{Av}$ and of $\{a+(b+a)K^2/[J(J+1)]\}$, the quadrupole and magnetic dipole coupling constants. The second expression given above for the value of $\langle eqQ\rangle_{Av}$ as a function of J and K seemed to fit our data best, and it was used to calculate the theoretical line frequencies listed in Table II. The first expression for $\langle eqQ\rangle_{Av}$ agrees better with the results of GM I at high values of J and K, but it increases some of the discrepancies between our own theoretical and experimental results for the case of the 1–1 line. It was, however, thought to be the best available compromise between the present work and that of GM I. The form of the dependence of $\langle eqQ\rangle_{Av}$ on J and K given in GM I was used simply because this form could not be well determined from the few lines which were measured under high resolution.

These results give a considerable amount of information about the electric and magnetic fields existing within the molecule, which should be explainable in terms of a satisfactory molecular theory. All three components of the molecular magnetic field at the position of the hydrogen nuclei are now known to good accuracy, as well as the two different components of the magnetic field and the gradient of the electric field at the position of the nitrogen nucleus, (which had been previously determined with good accuracy). Some discussion of the interpretation of these constants has been made in GM I.

One expects small variations of eqQ with J and K on account of the centrifugal distortion of the molecule, which produces changes in the inversion wave function. Similarly, a slight change in eqQ from upper inversion level to lower inversion level can be expected. The change of 4 kc/sec which explained satisfactorily the asymmetry of the 3–3 line was also applied on calculating the hyperfine structures of the other lines, but produced no changes in the spectra which would be detectable with the present apparatus. A remaining discrepancy which has not yet been explained is the apparent displacement of the main line of the 4–3 transition. Table II shows that the main line appears to be displaced by about 3 kc/sec away from the average frequency of the two inner quadrupole satellites. Since these measurements were taken rather carefully, this shift appears to be outside of experimental error. In this line the quadrupole splittings are small, so that the asymmetry cannot be accounted for by the small change in quadrupole coupling constant.

The change in eqQ from the upper state to lower can be qualitatively discussed with a relatively crude model. In the lower inversion state, the inversion wave function is a symmetrical function of z, the coordinate which

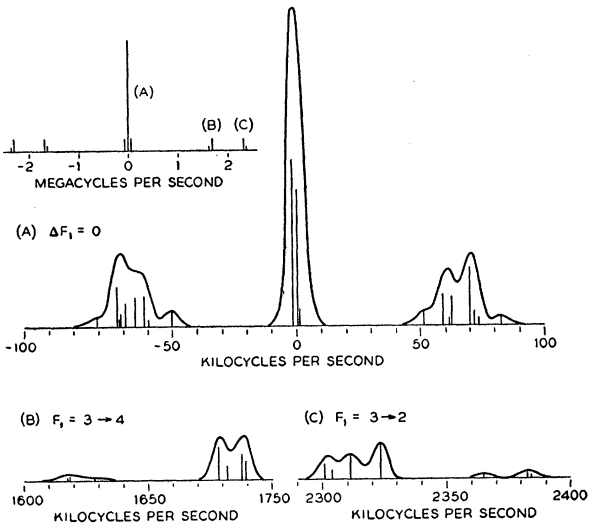

FIG. 5. Theoretical pattern of the hyperfine structure of the $J=K=3$ inversion transition. $\mathbf{F}_1=\mathbf{J}+\mathbf{I}_N$, where I_N is the spin of the nitrogen nucleus. The box at the upper left shows the complete spectrum. Below, the components (*a*), (*b*), and (*c*) of the complete spectrum are shown expanded. Frequency displacements from the position of a line undisplaced by hyperfine structure are shown on the figure. The positions and heights of the solid lines indicate the frequencies and intensities of the various hyperfine structure components of this transition. A total width at half-maximum of 7 kc/sec for each individual component was chosen to give a good fit to the observed spectrum. The intensity of the main line has been reduced by a factor of five.

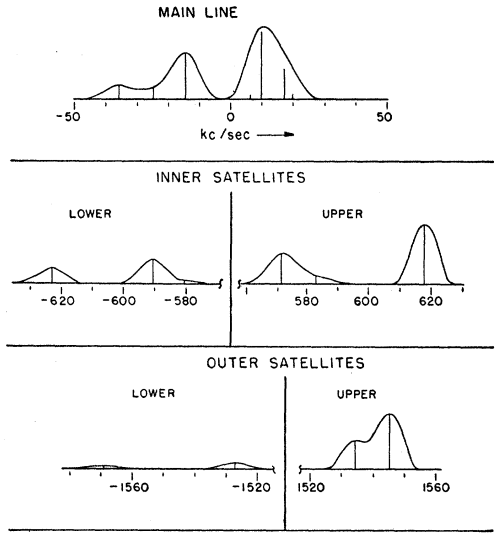

FIG. 6. Theoretical pattern of the $J=K=1$ inversion transition. Note that the symmetry of the hyperfine structure, which was evident in the 3,3 transition, is not present in this case. The total width at half-maximum of each hyperfine component of the transition is chosen as 10 kc/sec. Frequency displacements from the position of a line undisplaced by hyperfine structure are shown on the figure.

gives the position of the nitrogen nucleus on the symmetry axis of the molecule. In the upper state, the inversion wave function is an odd function of z. The nitrogen thus spends more of its time near the plane of the three hydrogens when the molecule is in the lower state. In its most probable configuration, the bond angles of the molecule are only slightly less than the tetrahedral angle. The quadrupole coupling constant is considerably smaller than would be expected if the five bonding electrons combined to form a completely covalent tetrahedral bond. This is due to the partially ionic character of the bond.[14] If, however, we neglect the ionic character and assume a completely covalent bond, we shall observe the proper trend in eqQ. For the tetrahedral bond, the two nonbonding electrons would be represented by $\frac{1}{2}s+\frac{1}{2}\sqrt{3}p_z$ hybrid orbitals, where z is the molecular axis. The value of $q_z=\partial^2V/\partial z^2$ at the position of the nitrogen may be considered as produced by only one of these nonbonding electrons, since the other plus the three bonding electrons form a symmetrical structure for which $q_z=0$. This results in a value $q_z=\frac{3}{4}q_p$, where q_p is the value of $\partial^2V/\partial z^2$ produced by a pure p_z orbital. For the planar configuration of the molecule, through which it must go while inverting, the three bonding electrons should be in sp^2 hybrid orbitals, while the two nonbonding electrons would both be in pure p_z orbitals. It can be shown that in this configuration $q_z=q_p$, which is larger in magnitude than that given by the tetrahedral structure. Thus one should expect the observed larger magnitude for quadrupole coupling in the symmetric lower inversion state, in which the nitrogen spends more time near the plane of the hydrogens.

APPENDIX. SIMPLIFICATION OF TERMS OF THE HAMILTONIAN INVOLVING THE OFF-AXIS NUCLEI

In the hyperfine structure problem in ammonia, one is frequently interested in matrix elements of the form

$$\langle\gamma JK|O|\gamma'J'K'\rangle, \tag{A1}$$

where O is a general operator which contains the spins of the hydrogen nuclei, and $J_z=K$. In other symmetric top molecules similar matrix elements will appear in which O contains the properties of the off axis nuclei. Some simplification of O may be effected by considering the symmetry properties of the molecule.

In the case of ammonia, the three hydrogen nuclei must obey Fermi-Dirac statistics, which means that any physically allowed state of the molecule must obey the equation

$$P_{ij}{}^{\sigma}P_{ij}{}^{x}|\psi\rangle=-|\psi\rangle \quad i\neq j, \tag{A2}$$

where $P_{ij}{}^{x}$ and $P_{ij}{}^{\sigma}$ represent exchange of space and spin coordinates, respectively, of hydrogen nuclei i and j. We shall find it to our advantage to confine our attention to those states of the molecule which satisfy the less restrictive equation

$$P_{ijk}{}^{\sigma}P_{ijk}{}^{x}|\psi\rangle=|\psi\rangle \quad i\neq j\neq k, \tag{A3}$$

where $P_{ijk}=P_{ij}P_{jk}$. States can be constructed satisfying Eq. (A3) which are separable into the product of a spin function and a space function and can be treated without difficulty.[15] The space functions are to be eigenfunctions of the angular momentum operator J_z, which commutes with both $P_{ijk}{}^{x}$ and $P_{ijk}{}^{\sigma}$. The final state function satisfying Eq. (A2) will of necessity be formed of linear combinations of functions satisfying Eq. (A3), so that no generality is lost in this procedure.

The operation $P_{123}{}^{x}$ is equivalent to a rotation of the molecule through an angle of $2\pi/3$ around its axis of symmetry, and thus can be written in the form $P_{123}{}^{x}=e^{\frac{2}{3}\pi iJ_z}$. Also $P_{123}{}^{\sigma}$ can be expressed in terms of the hydrogen spins I_i.[16] It has the effect of interchanging hydrogen spins; i.e., $(P_{123}{}^{\sigma})^{-1}\mathbf{I}_2P_{123}{}^{\sigma}=\mathbf{I}_1$, etc. In view of Eq. (A3) we may write

$$\begin{aligned}&\langle\gamma JK|O|\gamma'J'K'\rangle\\&=\langle\gamma JK|(P_{123}{}^{x})(P_{123}{}^{\sigma})^{-1}OP_{123}{}^{\sigma}P_{123}{}^{x}|\gamma'J'K'\rangle\\&=\langle\gamma JK|(P_{132}{}^{x})^{-1}(P_{132}{}^{\sigma})^{-1}OP_{132}{}^{\sigma}P_{132}{}^{x}|\gamma'J'K'\rangle.\end{aligned} \tag{A4}$$

Allowing only the P^x operators to operate on the state functions, and averaging the three resulting expressions gives

$$\begin{aligned}&\langle\gamma JK|O|\gamma'J'K'\rangle\\&\quad=\tfrac{1}{3}\langle\gamma JK|O+e^{\frac{2}{3}\pi i(K'-K)}P_{132}{}^{\sigma}OP_{123}{}^{\sigma}\\&\qquad+e^{-\frac{2}{3}\pi i(K'-K)}P_{123}{}^{\sigma}OP_{132}{}^{\sigma}|\gamma'J'K'\rangle.\end{aligned} \tag{A5}$$

In the particular case of ammonia we shall be interested in matrix elements diagonal in K and those joining the two degenerate states $+K$ and $-K$. Application of Eq. (A5) to the various interactions, particularly those diagonal in K, will reduce them to a simpler form.

We shall illustrate the method by applying it to the mutual spin-spin interaction of the hydrogens. This energy term [see Eq. (5)] transforms under rotations as a second degree spherical harmonic.[17] It can therefore have matrix elements joining state of $I=\frac{3}{2}$ to states of $I=\frac{3}{2}$ and $I=\frac{1}{2}$, but has no matrix elements joining two states of $I=\frac{1}{2}$. It will therefore contribute a term diagonal in K for the states with K a multiple of 3. All other nonzero matrix elements of this interaction (it can change J, K, F_1 by a maximum of two) are between states which are nondegenerate in the rotational energy, and so these matrix elements can be ignored. We are interested therefore only in matrix elements diagonal

[14] J. Bardeen and C. H. Townes, Phys. Rev. **73**, 97 (1948).

[15] For example, $P_{123}{}^{x}$ operating on the rotation vibration function $\psi_v{}^{JKM}$ multiplies it by $e^{i2\pi K/3}$. Thus we choose a spin function with the property that $P_{123}{}^{\sigma}$ operating on its multiplies it by $e^{-i2\pi K/3}$.

[16] P. A. M. Dirac, *The Principles of Quantum Mechanics* (Clarendon Press, Oxford, 1947), third edition, p. 222.

[17] J. H. Van Vleck, *Theory of Electric and Magnetic Susceptibilities* (Oxford University Press, London, 1932).

in K. Substituting $K'=K$ in Eq. (A5) gives

$$O \rightarrow \tfrac{1}{3}\{O+P_{132}{}^{\sigma}OP_{123}{}^{\sigma}+P_{123}{}^{\sigma}OP_{132}{}^{\sigma}\}. \quad \text{(A6)}$$

This operation immediately reduces (1) to (2) with only a small amount of algebra, after (1) is expanded in terms of the molecular axes.

To demonstrate the application of the method to interactions which have matrix elements of interest which are off-diagonal in K, we shall apply it to the hydrogen-nitrogen spin-spin interaction. This part of the Hamiltonian may be written

$$G^{\mathrm{HN}}=g_{\mathrm{H}}g_{\mathrm{N}}\mu_0{}^2r_{\mathrm{HH}}{}^{-3} \times\sum_i[\mathbf{I}_i\cdot\mathbf{I}_{\mathrm{N}}-3r_{\mathrm{HN}}{}^{-2}(\mathbf{I}_i\cdot\mathbf{r}_{i\mathrm{N}})(\mathbf{I}_{\mathrm{N}}\cdot\mathbf{r}_{i\mathrm{N}}), \quad \text{(A7)}$$

where r_{HN} is the hydrogen-nitrogen distance, and $\mathbf{r}_{i\mathrm{N}}$ is the vector distance between the ith hydrogen and the nitrogen. This interaction can lift the K degeneracy for $K=\pm1$, as shown in GM II, and so we shall be interested in the diagonal elements and those joining $K=\pm1$ to $K=\mp1$. Again, all other nonzero matrix elements are off-diagonal in the rotational energy. For the diagonal part we may make the substitution (A6), which here has the effect of replacing I_i by $I/3$, and so we obtain

$$\langle K|G_1{}^{\mathrm{HN}}|K\rangle=g_{\mathrm{H}}g_{\mathrm{N}}\mu_0{}^2\langle K|r_{\mathrm{HN}}{}^{-3}[\mathbf{I}\cdot\mathbf{I}_{\mathrm{N}} -\textstyle\sum_i r_{\mathrm{HN}}{}^{-2}(\mathbf{I}\cdot\mathbf{r}_{i\mathrm{N}})(\mathbf{I}_{\mathrm{N}}\cdot\mathbf{r}_{i\mathrm{N}})]|K\rangle. \quad \text{(A8)}$$

Expanding this in terms of the molecular axes then results in

$$\langle K|G_1{}^{\mathrm{HN}}|K\rangle=2g_{\mathrm{H}}g_{\mathrm{N}}v_0{}^2\langle K|r_{\mathrm{HN}}{}^{-3}(1-\tfrac{3}{2}\sin^2\beta) \times(I\cdot I_{\mathrm{N}}-3I_zI_{\mathrm{N}z})|K\rangle. \quad \text{(A9)}$$

Now we are here interested also in those matrix elements which join the two degenerate states of $K=\pm1$, so we must evaluate $\langle K=\pm1|G_1{}^{\mathrm{HN}}|K'=\mp1\rangle$. Application of (7) reduces this matrix to the form

$$\langle K=\pm1|G_1{}^{\mathrm{HN}}|K'=\mp1\rangle =g_{\mathrm{H}}g_{\mathrm{N}}\mu_0{}^2\langle K=\pm1|r_{\mathrm{HN}}{}^{-3}[-(9/4)\sin^2\beta \times(I_{1x}'\mp iI_{1y}')(I_{\mathrm{N}x}'\mp iI_{\mathrm{N}y}')]|K'=\mp1\rangle, \quad \text{(A10)}$$

or

$$\langle K=\pm1|G_1{}^{\mathrm{HN}}|K'=\mp1\rangle =g_{\mathrm{H}}g_{\mathrm{N}}\mu_0{}^2\langle K=\pm1|r_{\mathrm{HN}}{}^{-3}(9/2)\sin^2\beta \times(I_{1y}I_{\mathrm{N}y}-I_{1x}I_{\mathrm{N}x})|K=\mp1\rangle. \quad \text{(A11)}$$

Since (A9) and (A11) give all the matrix elements of interest, we see that the complete interaction can be replaced by the somewhat simplified form:

$$G_1{}^{\mathrm{HN}}\rightarrow g_{\mathrm{H}}g_{\mathrm{N}}\mu_0{}^2r_{\mathrm{HN}}{}^{-3}[(1-\tfrac{3}{2}\sin^2\beta)(\mathbf{I}\cdot\mathbf{I}_{\mathrm{N}}-3I_zI_{\mathrm{N}z}) +(9/2)\sin^2\beta(I_{1y}I_{\mathrm{N}y}-I_{1x}I_{\mathrm{N}x})]. \quad \text{(A12)}$$

Evaluation of the off-diagonal matrix elements (A11) may be made according to the standard methods of Condon and Shortley, remembering our choice of spin functions, or the equivalent Hamiltonian (A12) may be treated by the methods of GM II.

The method may easily be extended to the treatment of the $I\cdot J$ interaction, and yields the same result as that obtained in GM II. (Note the correction to GM II given in reference 8.)

ACKNOWLEDGMENTS

The author would like to express his appreciation to the personnel of the Columbia Radiation Laboratory who assisted in the construction of the experimental apparatus. Dr. H. J. Zeiger and Dr. T. C. Wang contributed greatly to the experiment in various stages. In particular the author is indebted to Professor C. H. Townes for suggesting this research and for his continued advice and guidance.

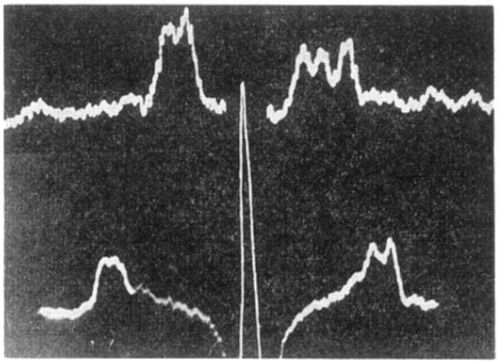

FIG. 4. Composite oscilloscope photograph of the $N^{14}H_3$ $J=K=3$ inversion transition at 23 870 Mc/sec. Below: main line with satellites caused by reorientation of the hydrogen spins. Above left: Inner quadrupole satellite, showing structure due to the hydrogens. Above right: outer quadrupole satellite. The main line has been retouched to make it more visible in the reproduction.